PCCP

Accepted Manuscript

ROYAL SOCIETY OF CHEMISTRY

www.rsc.org/pccp

Journal Name

RSCPublishing

ARTICLE

Cite this: DOI: 10.1039/x0xx00000x

Enhancement of Hydrogen Production Using Photoactive Nanoparticles on a Photochemically Inert Photonic Macroporous Support

Robert Mitchell,[a] Rik Brydson[b] and Richard E. Douthwaite[a]*

Received ooth January 2012,
Accepted ooth January 2012

DOI: 10.1039/x0xx00000x

www.rsc.org/

The propagation of light in photonic materials can be modified to increase the probability of photon absorption. Here we report the synthesis of composite materials comprising a photochemically inert photonic macroporous ZrO_2 support decorated with photocatalytically active CdS nanoparticles. The relative energies of valence and conduction bands restrict photon absorption and catalysis to the CdS nanoparticles. The generation of hydrogen from water under visible light illumination (>400 nm) has been studied as a function of the photonic support. A maximum 4.7 fold enhancement in hydrogen production is observed compared to a non-photonic support when the absorption band of the CdS nanoparticles partially overlaps with the blue edge of the photonic ZrO_2 stop band. This general strategy supports the independent optimization of optical and photochemical processes to increase the overall conversion efficiency of solar to chemical energy.

Introduction

The conversion of solar to chemical energy could provide a significant contribution to future energy needs if a viable process can be developed.[1-3] Many challenges remain, requiring the discovery of new materials and structures for light capture, charge separation and catalysis, and the integration of these phenomena into a functioning device.[4, 5] For light capture, the morphology of the absorbing material or structure supporting the light-active species is important to maximize absorption.[6]

3-dimensional macroporous photonic structures exhibit potentially useful phenomena for increasing the efficiency of solar energy conversion.[7, 8] Their periodic structure results in an ordered modulation of the refractive index between the material and voids, causing the propagation of light to be modified for specific frequencies.[9] Photonic materials are characterized by a stop band, which corresponds to frequencies that formally cannot propagate through the structure. The frequencies which respond to the photonic medium are determined by the composition and dimensions of the structure, providing the opportunity for predictable modification of the optical properties.[9]

In the context of solar energy conversion, macroporous photonic materials exhibit phenomena that have been shown to enhance the photon-to-electron conversion of photoelectrochemical devices at specific frequencies.[10-16] For example, a macroporous film of TiO_2 integrated into a dye-sensitized solar cell acts as a dielectric mirror to reflect light at the stop band and effectively increase the path length and probability of absorption.[10, 12] Enhancement can also result from a slowing of the photon group velocity at frequencies that overlap with the edges of the stop band, effectively increasing the path length.[17] For example, a macroporous photoelectrode of WO_3 exhibits over a 2-fold enhancement in photon-to-electron conversion at frequencies which overlap with the red edge of a stop band.[13] With respect to photochemical reactions, photonic macroporous TiO_2 has been shown to photocatalyze the degradation of an adsorbed dye monolayer.[18, 19] This work showed that materials with broad stop bands due to variations in periodicity can have practical application. Enhancement of photocatalytic hydrogen production from an aqueous methanol solution has also been demonstrated using platinum loaded macroporous TiO_2 and a macroporous WO_3 composite.[20, 21]

The synthesis of photonic photocatalysts is challenging for all but the simplest binary oxides. Our motivation was to prepare photoactive nanocrystals incorporated into a photocatalytically inert macroporous photonic host material and use the composite to mediate a photochemical reaction (Fig. 1). This general strategy allows potentially any photoactive material to be incorporated into a photonic host and the loading to be controlled. By varying the periodicity of the photonic host, the optical stop band can be positioned predictably with respect to the absorption band of the photoactive nanocrystals. Predictable colocation of the photonic support stop band and

photoactive nanocrystal absorption edge could lead to enhancement of, for example, hydrogen production from water under broad band visible light illumination, which is a key reaction for future solar fuel technology.

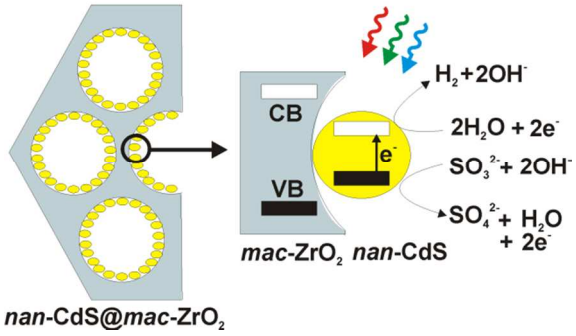

Fig. 1 Illustration of photocatalytically active CdS nanoparticles homogeneously coated onto a macroporous ZrO_2 support (left) and thier function (right). The relative energies of the conduction band (CB) and valence band (VB) of CdS in comparison to ZrO_2 restricts photoabsorption and redox catalysis to the CdS nanoparticles under visible light irradiation.

Experimental

Chemicals

Oleic acid ($C_{18}H_{34}O_2$, 90 %), styrene (C_8H_8, 99 %), potassium persulfate ($K_2S_2O_8$, 99 %), titanium tetraisopropoxide ($Ti(OC_3H_7)_4$, 97 %), polyvinylpyrrolidone (average molecular weight 40000), 1-octadecene ($C_{18}H_{36}$, 90 %), zirconium acetate solution in dilute acetic acid ($Zr[OCOCH_3]_4$, 16 % Zr), sodium sulfide nonahydrate ($Na_2S.9H_2O$, 98 %), sodium sulfite (Na_2SO_3, 98 %), tantalum oxide (Ta_2O_5, 99.99 %), cadmium oxide (CdO 99.99 %) and sulphur (reagent grade) were purchased from Sigma Aldrich and used as received.

Characterisation

SEM images were obtained using an FEI Sirion scanning electron microscope operating at 5 – 10 kV. Prior to imaging, samples were supported on an aluminium stub with an adhesive carbon tab and sputter coated with a 10 nm layer of carbon using an Agar auto carbon coater. Energy Dispersive Analysis of X-rays (EDX) was performed using an attached EDAX Phoenix X-ray spectrometer. TEM images were obtained using a JEOL 2011 transmission electron microscope operated at 200 kV accelerating voltage. TEM samples were ground, sonicated in methanol and a drop of the dispersion evaporated onto a holey carbon, copper grid. Electron diffraction and HAADF STEM imaging/EDX mapping were performed at the University of Leeds on a Tecnai TF20 FEGTEM. PXRD patterns were recorded on a Bruker-AXS D8 Advance instrument with Lynx eye detector, using Cu Kα radiation, scanning in the range 5 – 70 (2θ), with a 0.02 ° step size, and each data point collected for 0.05 or 0.1 s. Diffuse Reflectance UV spectra were recorded between two glass slides on an Ocean Optics HR2000+ High Resolution Spectrometer with DH-2000-BAL Deuterium/Helium light source (200 – 1100 nm). TGA analysis of *OA*-ZrO_2 samples was performed using a Rheometric Scientific STA-625 instrument. The weight loss of a sample was measured on heating to 600 °C at 10 °Cmin^{-1} under N_2 atmosphere. Nitrogen adsorption porosimetry was performed on a Micromeritics Tristar 3000 surface analyser. The sample was degassed under N_2 at 150 °C for 6 hr to remove all adsorbed water prior to measurement. The volume of nitrogen adsorbed at 77.4 K per gram of material was measured as a function of the relative pressure P/P0 within the system. Surface area measurements were calculated from data points in the 0.05 to 0.3 P/P0 region using the Brunauer Emmett Teller (BET) adsorption isotherm.[22]

Synthesis procedures

Polystyrene sphere templates were prepared using a modified literature procedure†.

***mac*-ZrO_2 (1 – 4):** *mac*-ZrO_2 was synthesised by a modified literature method.[9] Zirconium acetate in acetic acid (16 wt % Zr, 3 mL) and methanol (3 mL) were stirred for 15 min. The solution was transferred via pipette onto the polystyrene template (ca. 1 g) supported by a glass frit and allowed to soak for 1 h. Excess solution was then removed under reduced pressure. The impregnated template was dried at room temperature for 24 h prior to calcination at 450 °C (1 °C min^{-1}) for 4 h, to remove the template and yield *mac*-ZrO_2 (150-200 mg) as a coloured powder, dependent on the pore size.

Synthesis of *OAnan*-CdS: CdS nanocrystals were synthesised by a modified literature method.[23] CdO (38.4 mg, 0.30 mmol), oleic acid (2.5422 g, 9 mmol) and 1-octadecene (13.4194 g) were added to a 3 neck round bottom flask and heated to 300 °C under Ar. A solution of sulphur (4.8 mg, 0.15 mmol) in 1-octadecene (1.9952 g) was rapidly injected into the reaction mixture, and the temperature held at 270 °C for nanocrystal growth. After 180 s the reaction was quenched in an ice bath. The nanocrystals were precipitated by addition of excess ethanol followed by centrifugation (4400 rpm, 30 mins). The supernatant was discarded and the nanocrystals twice redispersed in toluene, precipitated with ethanol and isolated using a centrifuge (4400 rpm, 30 mins). On prolonged storage not all of the nanocrystals would dissolve, therefore the nanocrystals were dispersed and stored in toluene at a concentration of *ca.* 10 mgmL^{-1}. Elemental Analysis of the isolated nanocrystals Found (%) C 62.30; H 10.30; N 0; Calc. CdS:2.31 $C_{18}H_{34}O_2$.

Synthesis of *nan*-CdS@*mac*-ZrO_2 (1-CdS – 5-CdS): Macroporous materials (**1** – **4**) and commercial ZrO_2 (**5**) were initially coated with oleic acid by dispersing 40 mg of ZrO_2 in a hexane solution of oleic acid (0.05 M, 40 mL). After stirring for 3 h, the solid was collected by vacuum filtration and dried at 60 °C for 1 hr. The oleic acid content was 2.2 wt % determined by TGA (Fig S1a). To a 10 mm diameter glass vial was added 30 mg oleic acid coated ZrO_2 and 1.5 mL of a toluene stock solution of *OAnan*-CdS (10 mgmL^{-1}). To two separate vials was also added 1.5 mL of *OAnan*-CdS stock solution only. The

volatiles of all the vials were evaporated at 80 °C overnight to constant weight giving the mass of *OAnan*-CdS added to each vial 15.30 ± 0.30 mg. The *OAnan*-CdS@OA-ZrO_2 composites and control vials of *OAnan*-CdS were calcined at 450 °C for 4 hr with a heating rate of 1 °C min^{-1} to give *nan*-CdS@*mac*-ZrO_2 (**1-CdS – 4-CdS**), *nan*-CdS@ZrO_2 (**5-CdS**), and *nan*-CdS, respectively. Trace quantities of C, H and N were detected by combustion analysis and the control vials gave 2.80 ± 0.05 mg of CdS. The *nan*-CdS loading for **1-CdS – 5-CdS** is 9.5 wt% *nan*-CdS@*mac*-ZrO_2.

Synthesis of *OAnan*-TiO_2: Were prepared using a modified literature procedure.[24] Oleic acid (90 %, 35 g, 0.124 mol) was degassed under nitrogen in a 3-neck round bottom flask and heated to 100 °C. Titanium isopropoxide (2.84 g, 10 mmol) was added and the solution stirred for 5 min. Triethylamine (1.01 g, 10 mmol) in ethylene glycol (6.4 g, 0.103 mol) was subsequently added, and the mixture refluxed at 100 °C for 60 h. After cooling the solution, nanoparticles were precipitated by addition of excess ethanol (100 mL). Centrifugation (4000 rpm, 30 min) was used to isolate the nanoparticles, which were then washed twice with ethanol (40 mL) to remove residual surfactant to give an orange solid (2.1 g). The solid could be stored and later dispersed in 0.1 M oleic acid in chloroform. The average particle size determined by TEM was 8.9 ± 0.1 nm. Elemental Analysis of the isolated nanocrystals Found (%) C 62.6; H 9.72; N 0; Calc. $TiO_2.1.25C_{18}H_{34}O_2$.

Synthesis of *nan*-TiO_2@*mac*-ZrO_2 (1-TiO_2 – 5-TiO_2): The synthesis and characterisation of composites *nan*-TiO_2@*mac*-ZrO_2 have been reported previously.[25] Using a method analogous to **1-CdS – 5-CdS**, 70 mg of *OAnan*-TiO_2 dispersed in oleic acid in chloroform (0.1 M, 1 mL) by sonication was added to 15 mg of oleic acid coated ZrO_2 followed by evaporation of the volatiles at 40 °C over 2 hr. The composites were calcined at 450 °C for 4 hr with a heating rate of 1 °C min^{-1}) to give **1-TiO_2 – 5-TiO_2**. The *nan*-TiO_2 loading for **1-TiO_2 – 5-TiO_2** is 47 wt% *nan*-TiO_2@*mac*-ZrO_2.

Photocatalysis

The apparatus used for photoreaction and analysis of products has been described previously (Fig. S6a†).[26] For **1-CdS – 5-CdS**, reactions were performed in water (20 mL) containing Na_2S (0.25 M) and Na_2SO_3 (0.35 M) and 30 mg of the photocatalyst. The apparatus was maintained at a temperature of 40 °C. For **1-TiO_2 – 5-TiO_2**, reactions were performed in aqueous 10% MeOH with 23 mg photocatalyst to obtain comparable amounts of hydrogen as **1-CdS – 5-CdS**. Reactions were run three times giving data within 15 %. In addition, a control reaction using Ta_2O_5 (30 mg) in aqueous 10 % methanol was run periodically to monitor system calibration, which we have found is reproducible from batch to batch. Illumination was performed using a 300 W Xe lamp fitted with a 15 cm IR filter and a wideband $AlMgF_2$ coated mirror (irradiance 900 mWcm^{-2} measured using an International Light Technologies photometer, over the wavelength range 200 - 1100 nm). For CdS containing samples, a 400 nm band pass filter was used. All other reactions were performed without the filter. Gas analysis was performed using a Shimadzu Corporation GC-2014. Gases were separated on a 25 cm long column packed with 5 Å molecular sieves and detection was performed using a thermal conductivity detector (TCD). The gas samples were analysed using the following conditions; 20 mL/min flow rate of Ar gas, 90 °C column temperature and 120 °C detector temperature. Under these conditions the retention time of H_2 is 1.5 min.

Results and Discussion

Synthesis and Characterisation

The choice of photonic support was based on consideration of the optical and electronic properties, and chemical reactivity with respect to the photochemical reaction. An ideal material would have a large refractive index, wide band gap and be photochemically inert. A high refractive index is required because the photonic properties are characteristic of the difference in the refractive index between the material and voids. A wide band gap material will not absorb photons corresponding to visible wavelengths. Furthermore, where the valence and conduction bands of the photon absorbing species are within the valence and conduction bands of the support, the probability of charge transfer between the excited species and the support will be reduced (Fig. 1). In this study ZrO_2 was selected which has a refractive index of ca. 2.20 across visible wavelengths, a band gap of ca. 4 eV,[11] and does not corrode or catalyse photochemical reactions of water on illumination with the 300 W Xe arc lamp used here. In addition, synthesis of a photonic macroporous morphology has been described previously.[5]

$$\lambda_{max} = \frac{2d_{hkl}}{m}\left[\varphi n_{ZrO2} + (1-\varphi)n_{void}\right] \qquad \text{(Eqn. 1)}$$

The macroporous materials described here exhibit the inverse opal structure and the position of optical stop bands are given by Eqn. 1 which allows predictable modification of the stop band position. λ_{max} is the stop band maximum, n is the relative refractive indices of the void and wall materials, d_{hkl} is the void lattice plane spacing, φ is the volume of the wall or 'fill factor', and m is the Bragg plane order. It is therefore possible to determine the periodicity and fill factors required to obtain stop bands in positions that may modify the photochemical behaviour of a photoactive material contained within the photonic structure.

CdS was chosen as the photocatalytically active material because the photophysics and chemistry are well described. CdS also exhibits photocatalytic activity for the reduction of water to dihydrogen under visible light illumination.[27, 28]

Initially, four samples of macroporous ZrO_2 (*mac*-ZrO_2), with varying periodicity, were prepared using an established polystyrene templating method.[9] Scanning electron microscopy

(SEM) shows an ordered macroporous structure (Fig. 2) with periodicities of 165 (**1**), 255 (**2**), 270 (**3**), and 320 nm (**4**), respectively. Powder X-ray diffraction (PXRD) (Fig. S4a†) indicates that the macroscopic structure comprises nanocrystallites of tetragonal ZrO_2 approximately 5 nm in diameter and transmission electron microscopy (TEM) analysis gave 3.47 ± 0.33 nm. The surface areas determined from N_2 adsorption isotherms gave very similar values of 25 $m^2 g^{-1}$ for **1** – **4** (Fig. S7†).

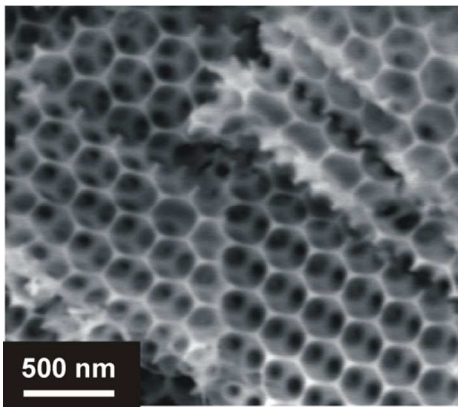

Fig. 2 SEM image of *mac*-ZrO_2 (**2**).

Diffuse reflectance UV-vis spectroscopy (DRUVS) (Fig. 3) showed characteristic stop bands, attributable to the 111 Bragg reflection, with λ_{max} = 500 (**2**), 535 (**3**) and 625 nm (**4**), respectively which lead to distinct colour in reflection (**1** = grey; **2** = blue; **3** = green; **4** = pale yellow) (Fig. S1b). In air, the stop band of **1** is predicted to be in the UV and is not observed. However, on filling the voids with water, the stop bands shift to longer wavelength, 430 (**1**), 625 (**2**), 675 (**3**) and 770 nm (**4**), respectively (Fig. S5a†), reflective of the refractive index difference (n_{air} = 1.00, n_{water} = 1.33) in accord with Eqn. 1. Fill factors φ = 16 - 17 % for **1** - **4**, are calculated using Eqn. 1, which is common for this class of material.

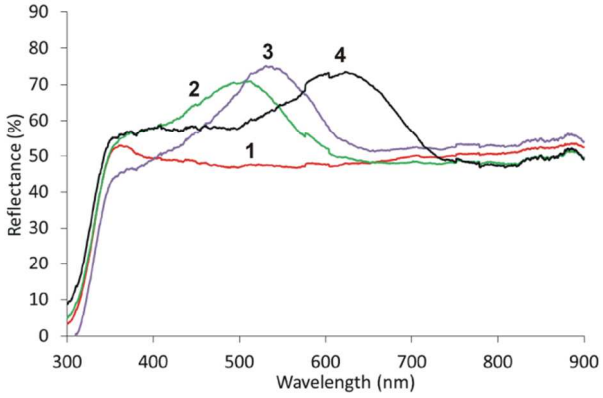

Fig. 3 DRUVS of **1**-**4** in air.

Prior to nanoparticle deposition, *mac*-ZrO_2 was coated with oleic acid (OA*mac*-ZrO_2).[25] Thermogravimetric analysis of OA*mac*-ZrO_2 showed a mass loss of 2.2 % (Fig S1a†), which corresponds to removal of a monolayer surface coating of oleic acid with an estimated footprint of 48 Å^2.[29] In the absence of an oleic acid coating, homogeneous nanoparticle deposition was not observed.

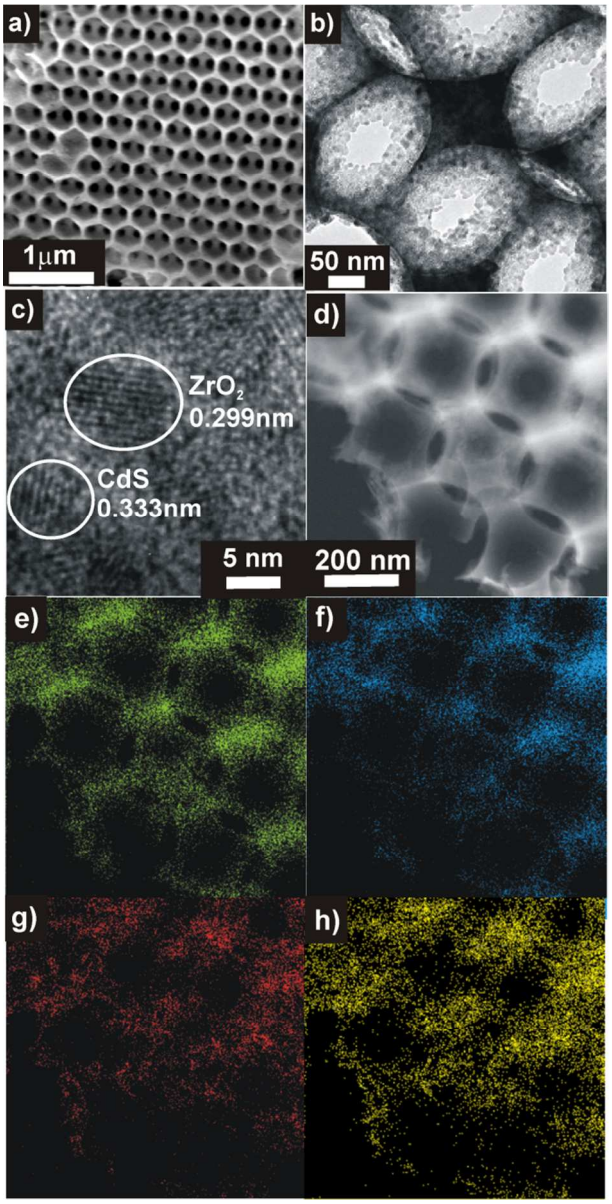

Fig. 4 a) SEM of **4-CdS**; b) TEM of **4-CdS**; c) Lattice fringes of individual nanoparticles. d) – h) HAADF STEM image and EDX maps; d) image; e) zirconium; f) oxygen; g) cadmium; h) sulfur.

Oleic acid stabilized nanoparticles of CdS (*OAnan*-CdS) were prepared independently to give particles of 2.84 ± 0.30 nm diameter as judged by TEM (Fig. S3a†) and are readily dispersed in common organic solvents.[23] Deposition of OA*nan*-CdS (9.5 wt% by CdS) from a toluene solution onto OA*mac*-

ZrO_2, followed by calcination at 400 °C gave the composites *nan*-CdS@*mac*-ZrO_2 (**1-CdS** – **4-CdS**). Combustion analysis of the composites showed that no carbon is present indicating the oleic acid ligands are removed on calcination. All the composites exhibit shades of orange coloration (Fig. S1c†) due to outer surface coverage by *nan*-CdS. SEM and TEM (Fig. 4a and 4b) indicate that aggregation of the nanoparticles does not occur. Elemental mapping using scanning TEM/energy dispersive X-ray analysis (EDX) (Fig. 4d – 4h) shows that nanoparticle coverage throughout the macroporous structure is homogeneous. In addition, DRUVS spectra (Fig. S5b†) do not show a significant decrease in intensity which also reflects homogeneous coverage.

$$\lambda_{max} = \frac{2d_{hkl}}{m}\left[\varphi n_{ZrO2} + \chi n_{CdS} + (1 - \varphi - \chi) n_{void}\right] \qquad \text{(Eqn. 2)}$$

The addition of *nan*-CdS is predicted to cause a red shift of the stop band λ_{max} commensurate with Eqn. 2, where χ is the volume fraction of *nan*-CdS.[25] Red shifts of 6-11 nm are observed for **1-CdS** – **4-CdS** which is consistent with the addition of 9.5 wt % of CdS (n = 2.4) to **1** – **4.** The volume fraction χ = 1.9 %, showing that the composite volume remains principally air as indicated by SEM (Fig. 4a).

For control experiments, a second series of composites containing anatase TiO_2 nanoparticles (*nan*-TiO_2) were deposited using an analogous method for **1-CdS** – **4-CdS** to give **1-TiO$_2$** – **5-TiO$_2$**. We have previously reported the detailed synthesis and characterisation of *nan*-TiO_2@*mac*-ZrO_2 composites.[25] Red shifts in the DRUVS data for the samples prepared here (Fig. S5d and S5e†) confirm the addition of TiO_2 and show that coverage is homogeneous, which was also supported by TEM.

Photocatalysis

Composites **1-CdS** – **4-CdS** were tested for hydrogen production from water under visible light illumination (>400 nm), in an aqueous solution of Na_2S and Na_2SO_3 as sacrificial reductants to prevent photocorrosion.[27] It should also be noted that the addition of metal cocatalyst nanoparticles (typically Pt) is also commonly used to increase the activity in photocatalytic hydrogen production of semiconductors, including CdS. In this study a cocatalyst was avoided because distribution of a second quantity of nanoparticles would complicate analysis. Furthermore Pt is known to cause photoetching of CdS.[27]

Data were compared against controls of **1** - **4**, and a commercial non-porous powder of ZrO_2 (**5**) decorated with 9.5 wt% *nan*-CdS (*nan*-CdS@ZrO_2 (**5-CdS**)). As a wide band gap semiconductor (4 eV), tetragonal ZrO_2 does not absorb significant photons above 400 nm and no hydrogen is evolved from **1** – **5**. In addition, for all samples no hydrogen was observed in the absence of light. However, hydrogen production is mediated by **1-CdS** – **5-CdS** under illumination with visible light (Fig. 5 and Table 1). For **2-CdS** the reaction was continued to give 2 equivalents of hydrogen with respect to CdS, indicating the reaction is catalytic. After an initial induction period hydrogen production is constant and remains so for subsequent reuse of **1-CdS** – **5-CdS**. For comparison, catalytic activity is often reported as hydrogen produced per gram of catalyst per hour ($\mu molg^{-1}h^{-1}$) although photoreactions are most commonly performed using much less than one gram of photocatalyst.[28] Composites **1-CdS** – **5-CdS** produce between 220 and 1083 $\mu molg^{-1}h^{-1}$ (Table 1) which is within the range reported for CdS photocatalysts of varying particle size and morphology including examples supported on metal oxides. Therefore the data in Table 1 supports the hypothesis that catalysis is limited to *nan*-CdS.[28]

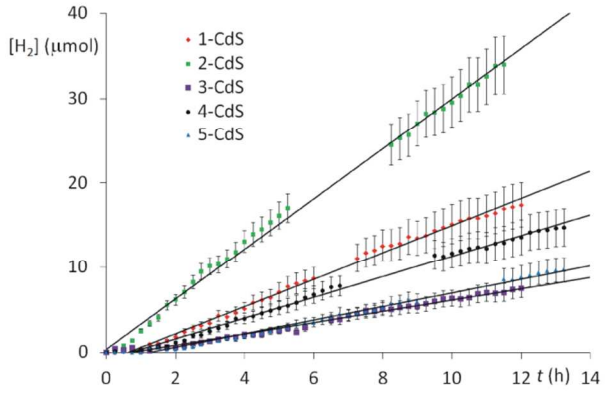

Fig. 5 Photocatalytic production of hydrogen using **1-CdS** – **5-CdS**.

Table 1. Photocatalytic hydrogen production for **1-CdS** – **5-CdS** and **1-TiO$_2$** – **5-TiO$_2$**.

Catalyst	Activity ($\mu molg^{-1}h^{-1}$)[a]	Catalyst	Activity ($\mu molg^{-1}h^{-1}$)[b]
1-CdS	450	**1-TiO$_2$**	261
2-CdS	1083	**2-TiO$_2$**	221
3-CdS	220	**3-TiO$_2$**	260
4-CdS	422	**4-TiO$_2$**	326
5-CdS	230	**5-TiO$_2$**	200

[a]Conditions: 30 mg catalyst (2.6 mg *nan*-CdS), 20 mL Na_2S (0.25 M) and Na_2SO_3 (0.35 M) in water, > 400 nm; [b]23 mg catalyst (7.4 mg *nan*-TiO_2), 20 mL10:90 methanol:water, > 325 nm.

The motivation for this work is the variation in hydrogen production of **1-CdS** – **5-CdS** as a function of the photonic properties. However, any observed variation could feasibly be attributable to reactant or product diffusion, catalyst dispersion, and surface area. Diffusion throughout inverse opal macroporous solids is unrestricted[30] and is irrelevant for powders such as **5-CdS**. The data is therefore not consistent with diffusion-limited photocatalysis, where **5-CdS** would be expected to exhibit the greatest activity. The dispersion of *nan*-CdS was determined using a combination of surface area measurements, TEM, and DRUVS. TEM and DRUVS data support homogeneous coverage (vide supra) and the surface area of **1** – **4** were found to be very similar (*ca.* 25 m^2 g^{-1}) and

significantly greater than the commercial ZrO_2 powder **5** (3 m^2g^{-1}) (Fig. S7†). Previous work has shown that addition of nanoparticles to macroporous ZrO_2 results in a small increase in surface area.[25] The quantity of nanoparticles added to **1-CdS** – **4-CdS** was identical, and therefore, the surface area and dispersion of *nan*-CdS does not account for the variation in hydrogen production.

With respect to optical phenomena, the DRUVS spectra for **1-CdS** – **5-CdS** after photocatalysis (Fig. 6) shows the onset of the absorption edge of *nan*-CdS at 520 nm, and stop bands from the photonic support. In comparison to **1** – **5** (Fig. 3) the position of the stop bands is consistent with the addition of 9.5 wt% *nan*-CdS and water to the pores as enumerated by Eqn. 2. An absorption edge of 520 nm is consistent with a band gap of 2.4 eV and indicates that *nan*-CdS does not exhibit quantum confinement behaviour that requires crystallites smaller than the Bohr radius of *ca.* 3 nm.[31] TEM shows a CdS particle size on the macroporous support of 3.51 ± 0.36 nm for **1-CdS** – **5-CdS**.

In the photocatalytic medium the composite **3-CdS** exhibits a stop band at a longer wavelength than the absorption of *nan*-CdS (Fig. 6). Therefore the photonic structure of the *mac*-ZrO_2 is not expected to significantly modify the photocatalytic behaviour of *nan*-CdS, and, as observed, in the absence of any other discriminating factors (*vide supra*) the photoactivity should be comparable to non-photonic **5-CdS**.

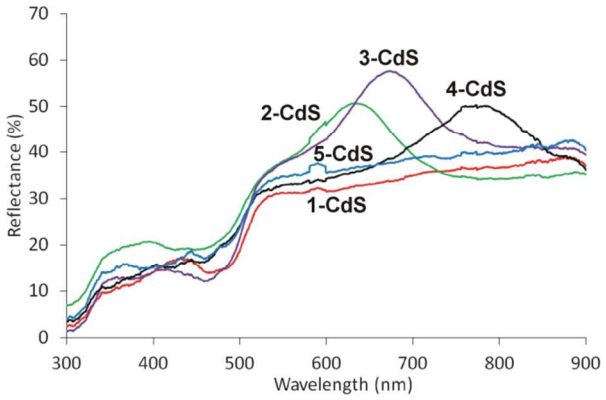

Fig. 6 DRUVS of **1-CdS** – **5-CdS** in aqueous Na_2S (0.25 M) and Na_2SO_3 (0.35 M) after photocatalysis.

In contrast, composites **1-CdS**, **2-CdS** and **4-CdS** all show greater activity than **3-CdS** and **5-CdS**. For **2-CdS**, the blue edge of the stop band partially overlaps the absorption edge of *nan*-CdS where slowing of the photons is expected to occur.[17] The enhanced hydrogen production observed for **2-CdS** is therefore consistent with a slowing of the photons in the region of overlap leading to increased absorption and greater photocatalytic activity. Composite **1-CdS**, exhibits a stop band within the region of high absorption by *nan*-CdS. Photonic TiO_2 and WO_3 materials have shown enhancement of the photon-to-electron conversion efficiency where a stop band is within the absorption band.[11, 13] This is attributed to slow photons at the stop band edges and scattering effects arising from imperfections of the photonic structure arising from the particulate composition.[18] However, enhancements less than a factor of 2 are typically found. A difference in enhancement is expected for photons slowed at the red and blue edges, respectively due to the opposing effects of greater transmission of low energy red photons[17] and greater internal scattering of high energy blue photons. However, where absorption is commensurate with the stop band, reflection of photons occurs about the stop band centre, reducing absorption. Therefore any enhancement due to slow photons and scattering is offset by reflection. For semiconductor photocatalysts, which absorb all photons above a bandgap threshold, overlap between the stop band blue edge and absorption edge is therefore required to maximize enhancement. For **4-CdS** the secondary 220 stop band centred at 470 nm (Fig. S5a†) would also exhibit similar phenomena attributable to **1-CdS**, and hence comparable enhancement is observed.

As a further control, an alternative photocatalyst was identified which was not expected to exhibit significant enhancement attributable to the photonic structure of **1** – **4**. We have previously reported the synthesis and characterisation of *nan*-TiO_2@*mac*-ZrO_2 composites,[25] where TiO_2 exhibits the anatase polymorph. TiO_2 is considered the prototypical photocatalyst, however TiO_2 is not photocatalytically active under visible light illumination. The absorption edge of anatase is at 380 nm and because the absorption edge is separated from the intense stop bands of **1** – **4**, the photonic properties of **1** – **4** are not expected to significantly modify TiO_2 light absorption. TiO_2 is known to photocatalyse hydrogen production in water under UV illumination using methanol as a sacrificial reductant.[32] Proton reduction and methanol oxidation redox reactions are not photoactiviated, in common with the Na_2S/Na_2SO_3 sacrificial oxidation reaction used for **1-CdS** – **5-CdS** photoreactions (*vide supra*). Therefore only photon absorption by TiO_2 could potentially be sensitive to the optical properties of the photonic host.

nan-TiO_2 was coated onto **1** - **5** to give **1-TiO_2** – **5-TiO_2** and to obtain comparable amounts of hydrogen for the TiO_2 and CdS composites a loading of 47 wt% TiO_2 was used. Lower loadings led to excessive reaction times and collecting comparable amounts of hydrogen allows the variation in hydrogen production of **1-CdS** – **5-CdS** and **1-TiO_2** – **5-TiO_2** to be conveniently compared. For **1-TiO_2** – **5-TiO_2** hydrogen production (Table 1 and Fig. S6b†) is shown to vary within a narrow range in contrast to **1-CdS** – **5-CdS** and the variation observed for **1-TiO_2** – **5-TiO_2** is close to the estimated error (Fig. S6b). The mismatch between the absorption edge of the TiO_2 photocatalyst and stop band edges of the photonic host precludes variation of UV photon absorption due to the photonic effects, an possible enhancement of hydrogen production due to increased photon absorption.

Collectively, the data show that the photoactivity of *nan*-CdS is increased between a factor of 1.8 to 4.7 in comparison to **5-CdS** depending on the relative position of *nan*-CdS

absorption edge and *mac*-ZrO_2 stop band. The variation in hydrogen production is predominantly attributable to the optical properties of the macroporous support.

Conclusions

The photochemical activity of nanoparticles can be modified within a chemically inert photonic host to increase the yield of hydrogen production under broad band illumination. The data are consistent with increased photon absorption due to the 'slow photon' effect induced by the photonic host. In these systems enhancement is maximized when the blue edge of the 111 stop band overlaps with the onset of the photocatalyst absorption. In contrast to photonic photocatalysts, decorating a photonic host with photoactive nanoparticles provides the opportunity to independently optimize optical enhancement and parameters more traditional to heterogeneous catalysis, including nanoparticle catalyst size and morphology,[33, 34] and support-nanoparticle interaction.[35]

Acknowledgements

This work was supported by The White Rose Consortium and The Centre for Low Carbon Futures. Characterization data was enabled via support from the EPSRC-funded Leeds EPSRC Nanoscience and Nanotechnology Equipment Facility (LENNF)(EP/K023853/1).

Notes and references

[a] Department of Chemistry, University of York, Heslington, York, YO10 5DD (UK) E-mail: richard.douthwaite@york.ac.uk

[b] Institute for Materials Research, School of Process, Environmental and Materials Engineering, University of Leeds, Leeds LS2 9JT (UK).

† Electronic Supplementary Information (ESI) available: [Full experimental and additional characterising data]. See DOI: 10.1039/b000000x/

1. N. S. Lewis and D. G. Nocera, *P. Nat. A. Sci. USA*, 2006, **103**, 15729.
2. R. E. Blankenship, D. M. Tiede, J. Barber, G. W. Brudvig, G. Fleming, M. Ghirardi, M. R. Gunner, W. Junge, D. M. Kramer, A. Melis, T. A. Moore, C. C. Moser, D. G. Nocera, A. J. Nozik, D. R. Ort, W. W. Parson, R. C. Prince and R. T. Sayre, *Science*, 2011, **332**, 805.
3. A. Harriman, *Philos. Trans. R. Soc. A-Math. Phys. Eng. Sci.*, 2013, **371**, 16.
4. M. G. Walter, E. L. Warren, J. R. McKone, S. W. Boettcher, Q. X. Mi, E. A. Santori and N. S. Lewis, *Chem. Rev.*, 2010, **110**, 6446.
5. I. McConnell, G. H. Li and G. W. Brudvig, *Chem. Biol.*, 2010, **17**, 434.
6. G. D. Scholes, G. R. Fleming, A. Olaya-Castro and R. van Grondelle, *Nat. Chem.*, 2011, **3**, 763.
7. F. Marlow, Muldarisnur, P. Sharifi, R. Brinkmann and C. Mendive, *Angew. Chem. Int. Edit.*, 2009, **48**, 6212.
8. A. Stein, B. E. Wilson and S. G. Rudisill, *Chem. Soc. Rev.*, 2013, **42**, 2763.
9. R. C. Schroden, M. Al-Daous, C. F. Blanford and A. Stein, *Chem. Mat.*, 2002, **14**, 3305.
10. S. Nishimura, N. Abrams, B. A. Lewis, L. I. Halaoui, T. E. Mallouk, K. D. Benkstein, J. van de Lagemaat and A. J. Frank, *J. Am. Chem. Soc.*, 2003, **125**, 6306.
11. M. El Harakeh and L. Halaoui, *J. Phys. Chem. C*, 2010, **114**, 2806.
12. S. Guldin, S. Huttner, M. Kolle, M. E. Welland, P. Muller-Buschbaum, R. H. Friend, U. Steiner and N. Tetreault, *Nano Lett.*, 2010, **10**, 2303.
13. X. Q. Chen, J. H. Ye, S. X. Ouyang, T. Kako, Z. S. Li and Z. G. Zou, *ACS Nano*, 2011, **5**, 4310.
14. L. W. Zhang, C. Baumanis, L. Robben, T. Kandiel and D. Bahnemann, *Small*, 2011, **7**, 2714.
15. S. K. Karuturi, C. W. Cheng, L. J. Liu, L. T. Su, H. J. Fan and A. I. Y. Tok, *Nano Energy*, 2012, **1**, 322.
16. K. Kim, M. J. Kim, S. I. Kim and J. H. Jang, *Sci Rep*, 2013, **3**, 8.
17. A. Imhof, W. L. Vos, R. Sprik and A. Lagendijk, *Phys. Rev. Lett.*, 1999, **83**, 2942.
18. J. I. L. Chen, G. von Freymann, V. Kitaev and G. A. Ozin, *J. Am. Chem. Soc.*, 2007, **129**, 1196.
19. J. I. L. Chen, E. Loso, N. Ebrahim and G. A. Ozin, *J. Am. Chem. Soc.*, 2008, **130**, 5420.
20. J. Liu, G. L. Liu, M. Z. Li, W. Z. Shen, Z. Y. Liu, J. X. Wang, J. C. Zhao, L. Jiang and Y. L. Song, *Energy Environ. Sci.*, 2010, **3**, 1503.
21. X. Cui, Y. Wang, G. Jiang, Z. Zhao, C. Xu, Y. Wei, A. Duan, J. Liu and J. Gao, *RSC Adv.*, 2014, **4**, 15689.
22. S. Brunauer, P. H. Emmett and E. Teller, *J. Am. Chem. Soc.*, 1938, **60**, 309.
23. W. W. Yu and X. G. Peng, *Angew. Chem. Int. Edit.*, 2002, **41**, 2368.
24. P. D. Cozzoli, A. Kornowski and H. Weller, *J. Am. Chem. Soc.*, 2003, **125**, 14539.
25. R. Mitchell, R. Brydson and R. E. Douthwaite, *Nanoscale*, 2014, **6**, 4043.
26. N. S. Hondow, Y. H. Chou, K. Sader, R. Brydson and R. E. Douthwaite, *J. Phys. Chem. C*, 2010, **114**, 22758.
27. N. Buhler, K. Meier and J. F. Reber, *J. Phys. Chem.*, 1984, **88**, 3261.
28. K. Zhang and L. J. Guo, *Catal. Sci. Technol.*, 2013, **3**, 1672.
29. I. Langmuir, *P. Nat. A. Sci*,. 1917, **3**, 251.
30. T. Cherdhirankorn, M. Retsch, U. Jonas, H. J. Butt and K. Koynov, *Langmuir*, 2010, **26**, 10141.
31. A. D. Yoffe, *Adv. Phys.*, 1993, **42**, 173.
32. X. B. Chen, S. H. Shen, L. J. Guo and S. S. Mao, *Chem. Rev.*, 2010, **110**, 6503.
33. B. R. Cuenya, *Accounts Chem. Res.*, 2013, **46**, 1682.
34. S. Fukuzumi and Y. Yamada, *ChemSusChem*, 2013, **6**, 1834.
35. S. Schauermann, N. Nilius, S. Shaikhutdinov and H. J. Freund, *Accounts Chem. Res.*, 2013, **46**, 1673.